Supporting Information

Sulfur-regulated $CoSe_2$ Nanowires with High-charge Active Center for Electrochemical Nitrate Reduction to Ammonium

Wuyong Zhang; Yingjie Wen; Haocheng Chen; Minli Wang; Caihan Zhu; Yunan Wang; Zhiyi Lu**

Experimental details

Reagents: Cobalt nitrate hexahydrate ($Co(NO_3)_2·6H_2O$), ethylenediamine (EDA), cobalt powder (Co), sublimed sulfur (S), selenium powder (Se), potassium sulfate (K_2SO_4), potassium nitrate ($K^{14}NO_3$, $K^{15}NO_3$ 99.9%), diaminomaleonitrile salicylic acid ($C_7H_6O_3$, 99.9%), potassium sodium tartrate ($NaKC_4H_4O_6·4H_2O$, 99.9%), ammonium chloride (NH_4Cl, 99.98%), hydrochloric acid (HCl, 99.999% metal base), sodium hypochlorite (NaClO, available chlorine 6-14 %), para-(dimethylamino) benzaldehyde ($C_9H_{11}NO$, 99.9%) were purchased from Alfa Aesar. Standard NH_4^+-N solution (6 mg L^{-1}) and NO_2^--N solution (40 mg L^{-1}) were purchased from Merck. Unless otherwise stated, ultrapure (18.2 MΩ·cm) water was used in all experiments. All chemicals were used without further purification.

Synthesis of S-$CoSe_2$ NWs: S-$CoSe_2$ NWs was prepared by a solvothermal method. In a typical solvothermal preparation process, S (1 mmol), $Co(NO_3)_2·6H_2O$ (0.2 mmol) and Se (1 mmol) was dissolved in EDA (10 mL), followed by sonicating for 30 min. The above mixture was transferred to 60 mL Teflon-lined stainless-steel autoclave and heated to 170 °C for 18 h with a heating rate of 5 °C min^{-1}. The obtained black precipitates were collected by centrifugation, washed three times with water and ethanol, and finally dried in an oven at 80 °C overnight for further use without any

additional processing. The S-CoSe2 materials with different sulfur content can be regulate by the usage of sulfur.

Synthesis of $CoSe_2$ NSs: The similar synthesis process as for S-$CoSe_2$ NWs has been applied but sulfur is absent in this process. The morphology evolution process of CoSe2 are also regulated by the addition of sulfur.

Synthesis of Bulk $CoSe_2$: The bulk $CoSe_2$ was synthesized by solid-state reactions.[1] Typically, the cobalt powder and selenium powder mixture in a stoichiometric ratio was ground and then collected in a fused silica tube under vacuum, which was heated to 500 °C for 2 h at a rate of 50 °C h^{-1} and then heated at the same rate to 650 °C. After sintering at 650 °C for 12 h, the obtained samples were cooled to room temperature over 12 h.

Characterizations:

Scanning electron microscopy (SEM) was carried out on a Hitachi S-4800 operating at 10.00 kV. A thin platinum layer of a few nanometers thickness was sputter onto the surface of the samples to increase the surface conductivity. Energy-dispersive X-ray (EDX) investigations were conducted using a Link ISIS-300 system equipped with a Si (Li) detector and an energy resolution of 133 eV.

Transmission electron microscopy (TEM) and high-resolution transmission electron microscopy (HRTEM) was performed on a JEOL F200 microscope at an acceleration voltage of 200 kV. **The aberration-corrected high-angle annular dark-field scanning transmission electron microscopy (AC HAADF-STEM)** images were acquired using a double-Cs-corrected JEOL Spectra 300, equipped with a cold field emission gun and an acceleration voltage set to 80 kV. The microscope is further equipped with a double F200 energy-dispersive X-ray detector, which was utilized for the EDX measurements.

Atomic force microscope (AFM) was performed on a Veeco DI NanoScope MultiMode V system.

Powder X-ray diffraction (PXRD) patterns were recorded on a Bruker D8 Advance diffractometer equipped with a scintillation counter detector with Cu Kα radiation (λ = 0.15184 nm) applying 2θ step size of 0.025°.

X-ray photoelectron spectroscopy (XPS) data were obtained on AXIS SUPRA with a Physical Electronics spectrometer in fixed analyzer transmission mode using monochromatic Al K_α radiation ($h\upsilon$ = 1486.6 eV, spot diameter 200 μm and a power of 50 W) at an angle of 45° with a pass energy of 23.50 eV (step size of 0.1 eV) for region scans. The samples have been measured on indium foils and due to the good conductivity, no charge neutralization has been applied.

N_2 physisorption were performed at -196 °C on a Specific surface area and porosity analyzer (ASAP 2020). Prior to all the physisorption measurements, the samples were outgassed under vacuum at 140 °C for overnight. Specific surface areas (SSA) of the materials are calculated by using the multipoint Brunauer-Emmett-Teller (BET) model in the relative pressure range 0.05-0.2. The total pore volumes (V_t) were determined at p/p_0 = 0.99. The pore size distributions are calculated by using the quenched solid density functional theory (QSDFT) method for nitrogen on carbon with slit/cylindrical/spherical pores at -196 °C, adsorption branch kernel, integrated into the QuadraWin 5.11 analysis software (Quantachrome).

Thermal Gravimetric Analysis (TGA) were collected on a thermo microbalance STA 449F3. A platinum crucible was used for the measurement of 10 ± 1 mg of samples in a N_2 flow of 10 mL min^{-1} and a purge flow of 10 mL min^{-1}. The samples were heated to 1000 °C with a heating rate of 5 °C min^{-1}. The data was recorded and analyzed by the Proteus (6.0.0) and Quadstar (7.03) software package.

Nuclear Magnetic Resonance (NMR) spectra were obtained on a Bruker AVANCE III 600 MHz.

UV-vis spectra have been measured on a UV/VIS Spectrometer (TU-1810SPC, PERSEE). The scan rate and slit width were set to 100 nm min^{-1} and 0.5 mm, respectively.

In situ diffuse Fourier transform infrared spectroscopy (DRIFTS) was conducted on NICOLET 6700 (Thermo) with a cell accessory (LingLu) connected to an electrochemical setup. The catalyst was drop wised onto a single bounce silicon crystal covered with an Au membrane which prepared by the following process: (1) Monocrystal silicon was immersed in aqua regia for 20 min and then polished using

Al_2O_3 powder for 10 min. After washing three times with water and acetone, clean monocrystal silicon was obtained. (2) The above monocrystal silicon was immersed in 40% NH_4F solution and washed three times with water, then the modified monocrystal silicon was immersed into a solution (100 mL) containing NaOH (0.12 g), $NaAuCl_4 \cdot 2H_2O$ (0.23 g), NH_4Cl (0.13 g), Na_2SO_3 (0.95 g) and $Na_2S_2O_3 \cdot 5H_2O$ (0.62 g) for 5 min under 55 ^oC.

In situ Raman spectroscopy was conducted on confocal Micro-Raman (Renishaw inVia Reflex, Renishaw) with a homemade cell connected to an electrochemical setup. The working electrode was regulated to be the position between electrolyte and air to ensure the enough laser intensity, platinum wire and AgCl/Ag were used as counter electrode and reference electrode, respectively. Raman Microscope operates with an objective (Nikon, 50x/0.25, ∞/- WD 6.1) and an excitation wavelength of 532 nm with an intensity of 1 mW, the integral time is 30s for every given potential with three times. **The obtained XAFS data** was processed in Athena (version 0.9.26) for background, pre-edge line and post-edge line calibrations.[2] Then Fourier transformed fitting was carried out in Artemis (version 0.9.26). The k^3 weighting, k-range of 2-12 $Å^{-1}$ and R range of 1 - 3 Å were used for the fitting. The four parameters, coordination number, bond length, Debye-Waller factor and E_0 shift (CN, R, σ^2, ΔE_0) were fitted without anyone was fixed, constrained, or correlated. For Wavelet Transform analysis, the $\chi(k)$ exported from Athena was imported into the Hama Fortran code. The parameters were listed as follow: R range, 1-4 Å, k range, 0-12 $Å^{-1}$; k weight, 2; and Morlet function with κ=10, σ=1 was used as the mother wavelet to provide the overall distribution.

Electrochemical measurements:

The measurements were conducted on an CHI electrochemical setup (CHI 760e, Metrohm) with a three-electrode system. The counter electrode and reference electrode were platinum foil (1*1 cm^2) and a saturated calomel electrode (SCE), respectively. All potentials in this work are referred to RHE via the correction (0.059*pH+0.242) V. 0.5

M K_2SO_4 and 0.5 M K_2SO_4+0.5M KNO_3 aqueous solutions were prepared with ultrapure water from Millipore system and used as electrolytes. Electrolysis was performed in a H-type cell separated by Nafion membrane. Prior to the test, the Nafion membrane was pretreated by heating in 0.5 M H_2SO_4, ultrapure water, 5% H_2O_2 aqueous solution, and ultrapure water at 80 °C for 30 mins in turn. Linear sweep voltammetry (LSV) tests were conducted in Ar-saturated solution with a scan rate of 1 mV s^{-1}, the purity of the gas used in all experiments is 99.999%. The potentiostatic test was carried out at different potentials for 2 h. FE of the ammonia formation was calculated from the percentage of the total amount of the charge consumed for the production of ammonia (n_{NH_3}) in the total charge Q (C) passed through the electrochemical system. Since eight electrons are transferred for the formation of one ammonia molecule with dinitrogen molecule, the FE can be calculated as follows: FE= n_{NH_3}*8F/(I*t), where the F is the Faraday constant (96485.34 C mol^{-1}), I (A) is the current at the potential applied on the electrochemical system, and t (s) is the electrolysis time. The FE of the possible nitrite byproduct has been calculated in the same way but with counting two transferred electrons.

Detection of NARR products:

The concentrations of ammonium and nitrite in the electrolyte were analyzed with UV-vis spectroscopy and quantified based on the recorded standard curves. Before testing, the electrolyte was diluted in different ratios for some samples to fit the UV-vis calibration range depending on the concentration of ammonium/nitrite in the electrolyte after reaction.

For ammonium,[3] 2 mL diluted electrolyte was mixed with 2 mL chromogenic reagent of 1 M NaOH solution (containing 5 wt% of salicylic acid and 5 wt% of sodium citrate), followed by adding 1 mL oxidizing solution of 0.05 M NaClO and 0.2 mL catalyzing reagent of 1 wt% sodium nitroferricyanide. After standing at room temperature for 1 h, the produced indophenol blue was detected by UV-vis spectroscopy. The standard curve was plotted with the absorption intensity at 655.5 nm and the concentration of

standard NH_4^+ solution. The ammonia production is also proved by ^1H NMR with the internal standard method. Maleic acid ($C_4H_4O_4$) was selected as the internal standard with DMSO-d_6 as the deuterated solvent (20 mg $C_4H_4O_4$ dissolved in 50 g DMSO-d_6). Before the test, a series of NH_4^+ solution (450 μL, 0.5 M KNO_3+0.5 M K_2SO_4, pH=2) with different concentration was prepared and mixed with DMSO-d_6 (100 μL with internal standard inside) for the NMR test. The calibration curve was plotted by the peak integral area of NH_4^+ and corresponding concentrations. It is worth mentioning that the pH of solution should be adjusted to two with concentrated hydrochloric acid before test and the test process of NARR samples is same with that for recording the calibration curve. The ammonium concentration in the NARR electrolyte sample can then be calculated by the calibration curve.

For nitrite,[4] 0.2 g of N-(1-naphthyl) ethylenediamine dihydrochloride, 4 g of p-aminobenzenesulfonamide, and 10 mL of phosphoric acid (ρ = 1.685 g mL^{-1}) were added into 50 mL of deionized water and mixed thoroughly as the coloring reagent. 5 mL of the diluted electrolyte which fits the UV-vis testing range and 0.1 mL of color reagent were mixed together. After 20 min at room temperature, the UV-vis absorption spectrum was measured and the absorption intensity was recorded at a wavelength of 500 nm. A series of standard NO_2^--N solutions were used to obtain the concentration-absorbance curve by the same processes.

Isotope Labeling Experiments were performed with $K^{15}NO_3$ as N-source for the potentiostatic test. After electrolysis, the pH of electrolyte was adjusted to two by concentered HCl for further analysis by ^1H NMR (600 MHz).

Computational details:

All the DFT calculations are performed by the Vienna Ab initio Simulation Package (VASP) with the projector augmented wave (PAW) method.[5, 6] The exchange-functional is treated using the generalized gradient approximation (GGA) with Perdew-Burke-Ernzerhof (PBE) functional. The energy cutoff for the plane wave basis expansion was set to 400 eV.[7] Partial occupancies of the Kohn−Sham orbitals were

allowed using the Gaussian smearing method and a width of 0.2 eV. 2 ×2 ×1 supercell models for (210) and (311) facets were constructed in terms of the relaxed $CoSe_2$. The slabs were separated by a 15 Å vacuum layer and were added along the c direction to avoid the interaction between periodic images. The structure of $CoSe_2$(210) and S-$CoSe_2$ were optimized using the k-point of 2×2×1. The self-consistent calculations apply a convergence energy threshold of 10^{-5} eV, and the force convergency was set to 0.05 eV/Å. The transition state was located using the constrained optimization, where the force convergency was set to 0.05 eV/Å.[8]

The free energy corrections were considered at the temperature of 298 K, following:

$\Delta G = \Delta E + \Delta G_{ZPE} + \Delta G_U - T\Delta S$

where ΔE, ΔG_{ZPE}, ΔG_U, and ΔS refer to the DFT calculated energy change, the correction from zero-point energy, the correction from inner energy and the correction from entropy.[9]

Supplementary Figures

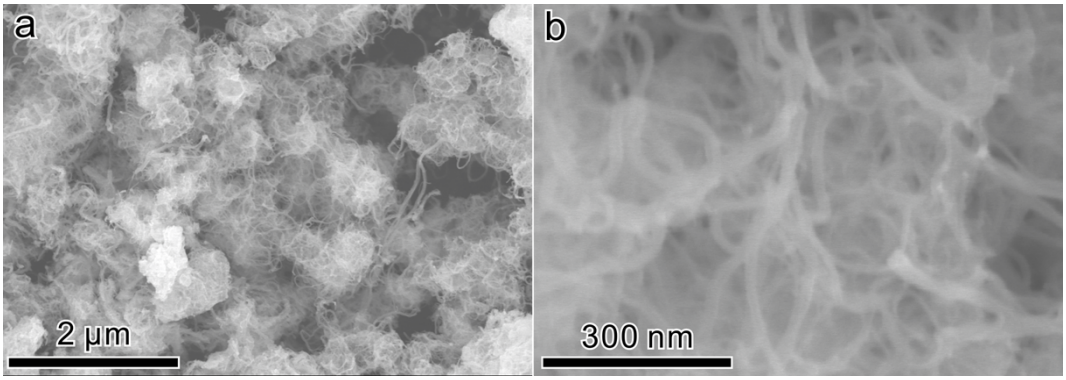

Figure S1. SEM images of S-$CoSe_2$ NW with different magnification.

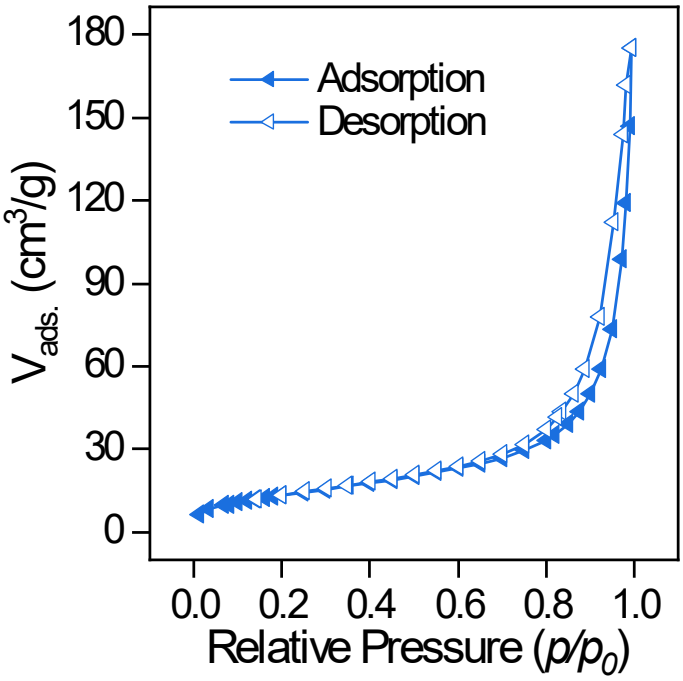

Figure S2. N_2 physisorption isotherms (at -196 °C) of S-$CoSe_2$ NWs.

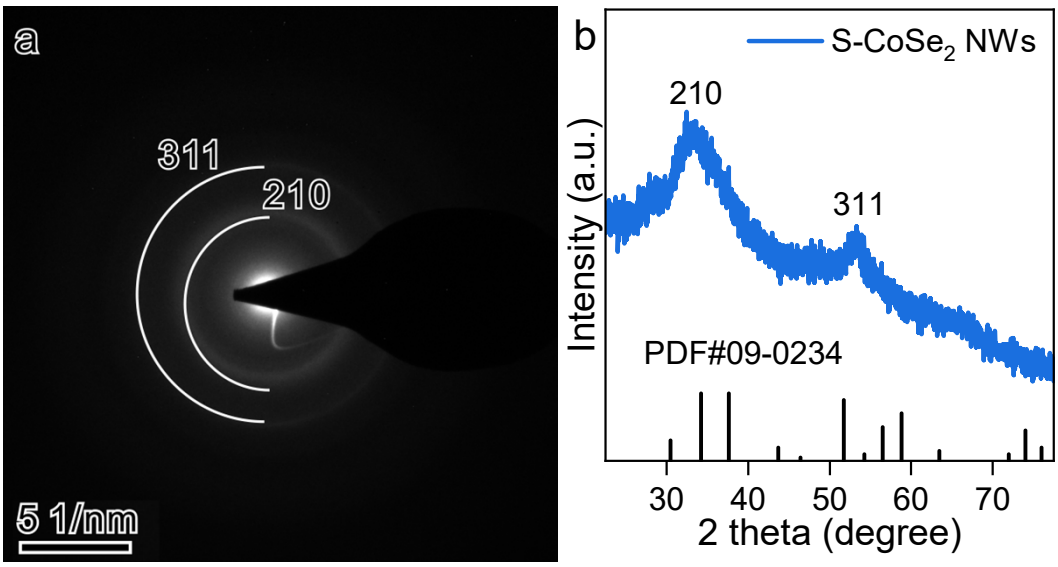

Figure S3. (a) SAED and (b) XRD pattern of S-$CoSe_2$ NWs.

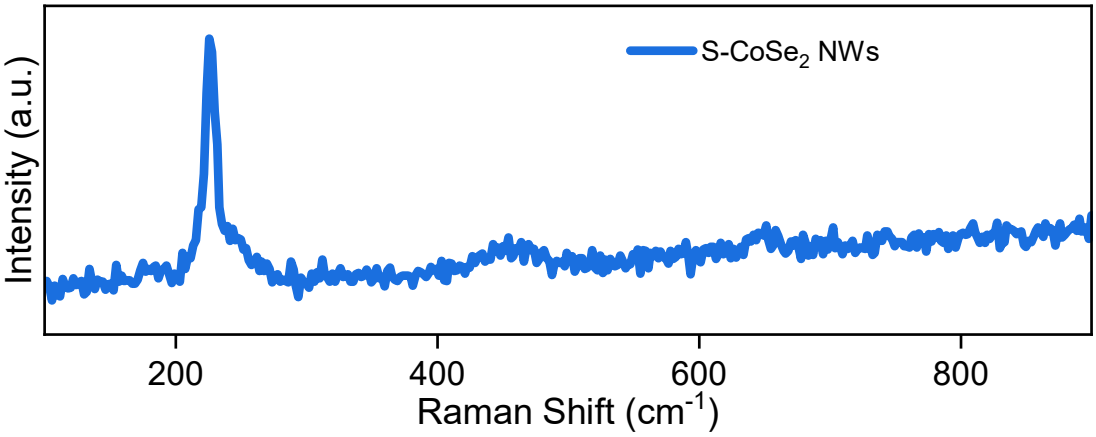

Figure S4. Raman spectrum of S-$CoSe_2$ NWs.

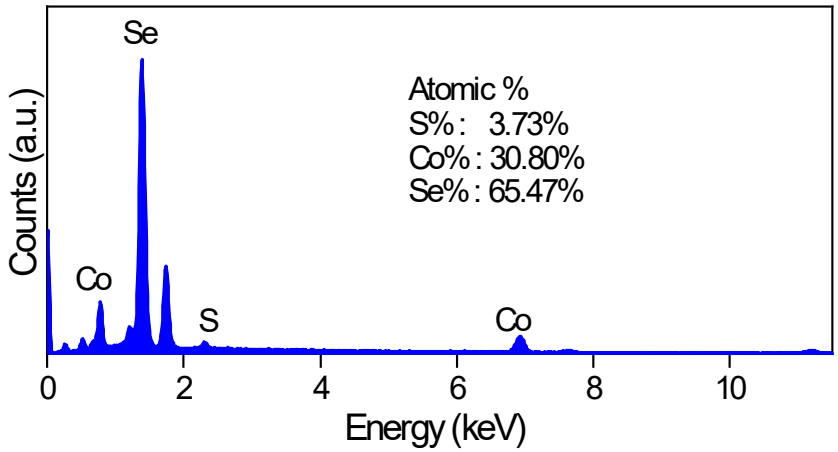

Figure S5. EDX spectrum of S-$CoSe_2$ NWs.

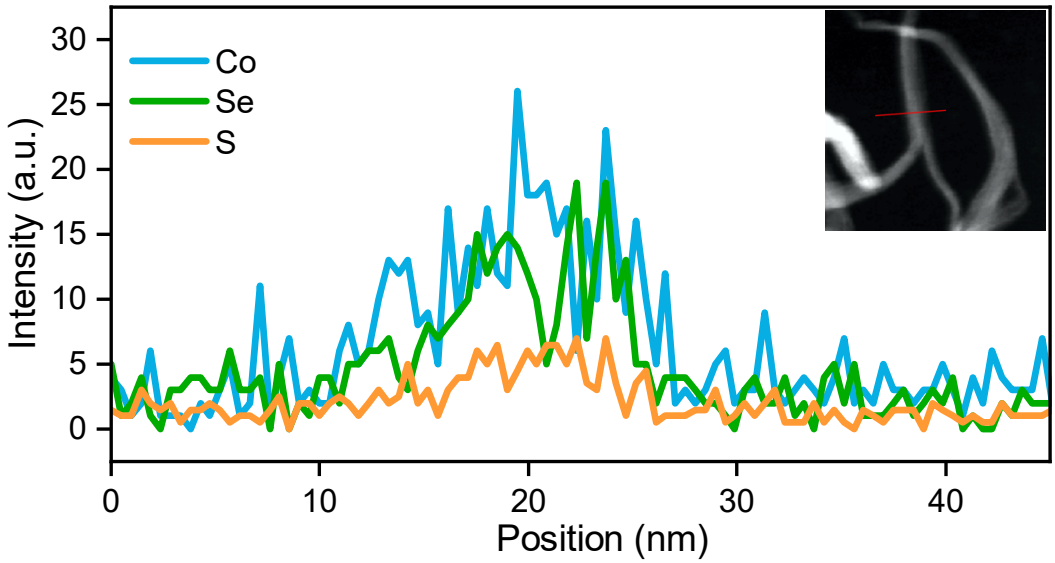

Figure S6. EDX line scanning images and corresponding elements profile of S-$CoSe_2$ NWs.

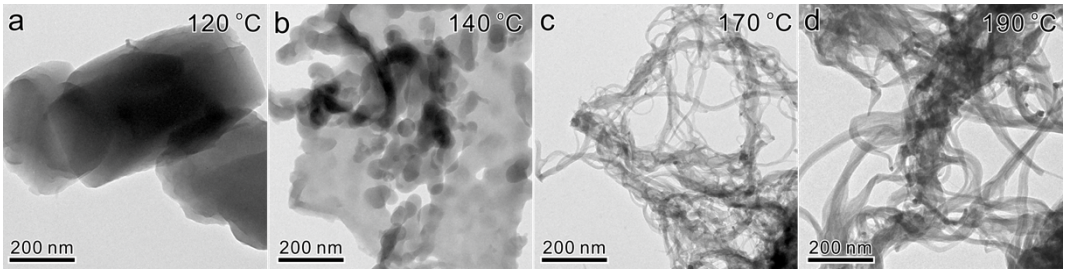

Figure S7. The TEM images of S-$CoSe_2$ products under different reaction temperature.

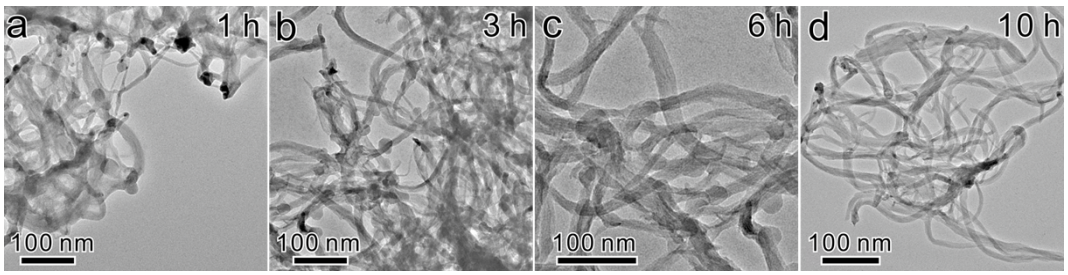

Figure S8. Time-dependent TEM images of S-$CoSe_2$ products.

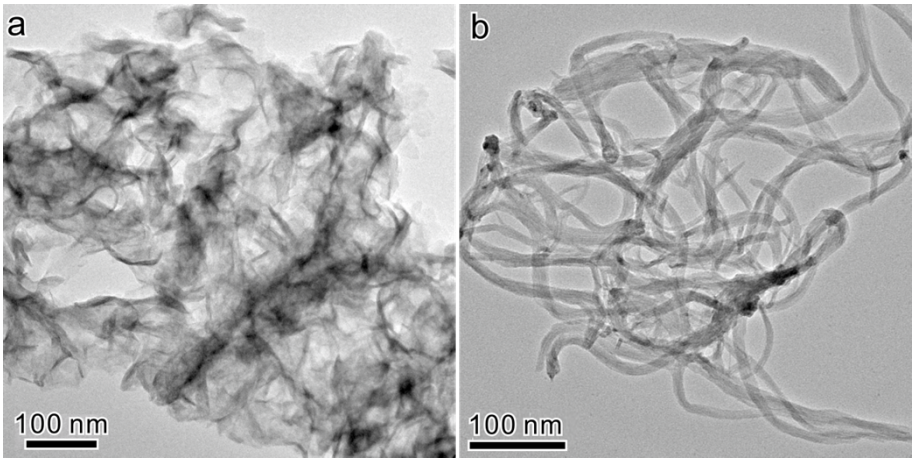

Figure S9. TEM images of (a) $CoSe_2$ NSs and (b) S-$CoSe_2$ NWs.

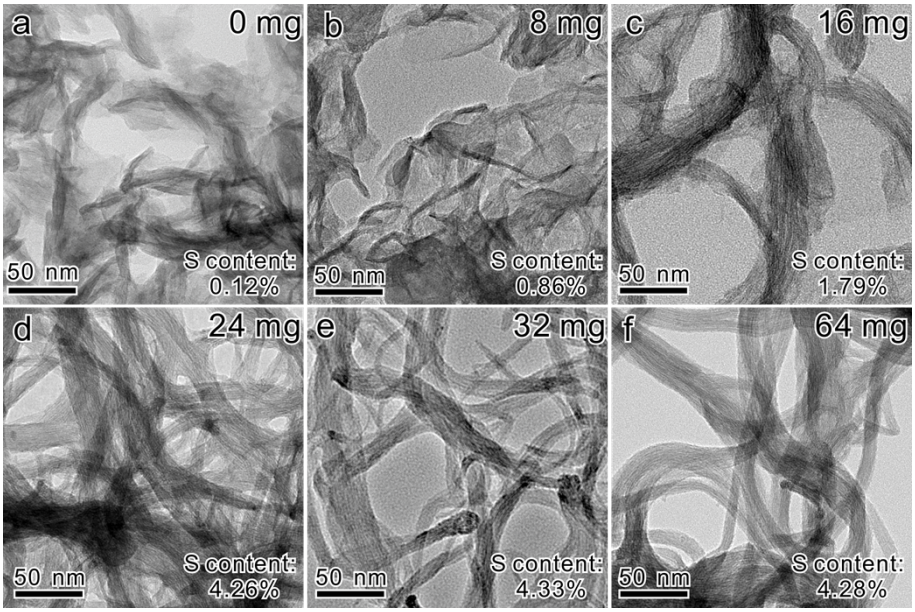

Figure S10. The morphology evolution of $CoSe_2$ with the regulation of sulfur usage when $Co(NO_3)_2$ $6H_2O$ usage is 58 mg.

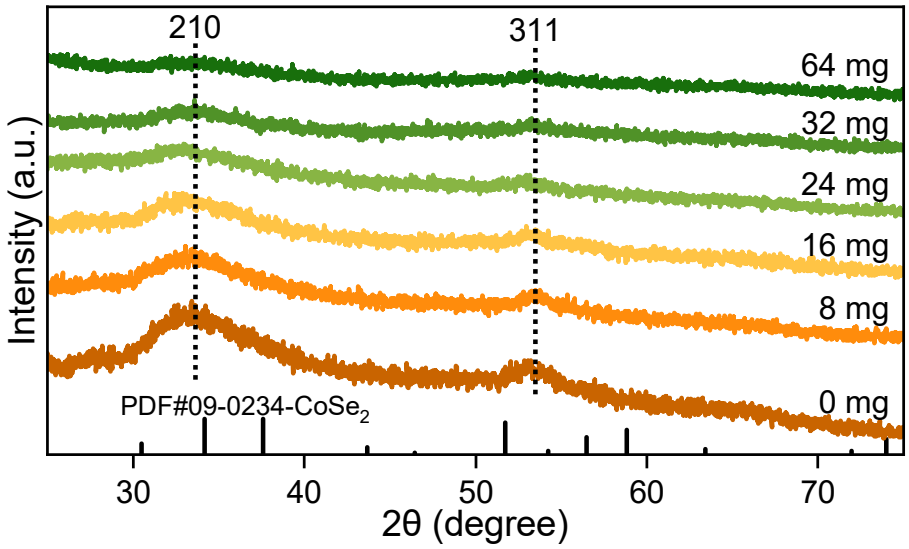

Figure S11. The XRD patterns evolution of $CoSe_2$ with the regulation of sulfur usage.

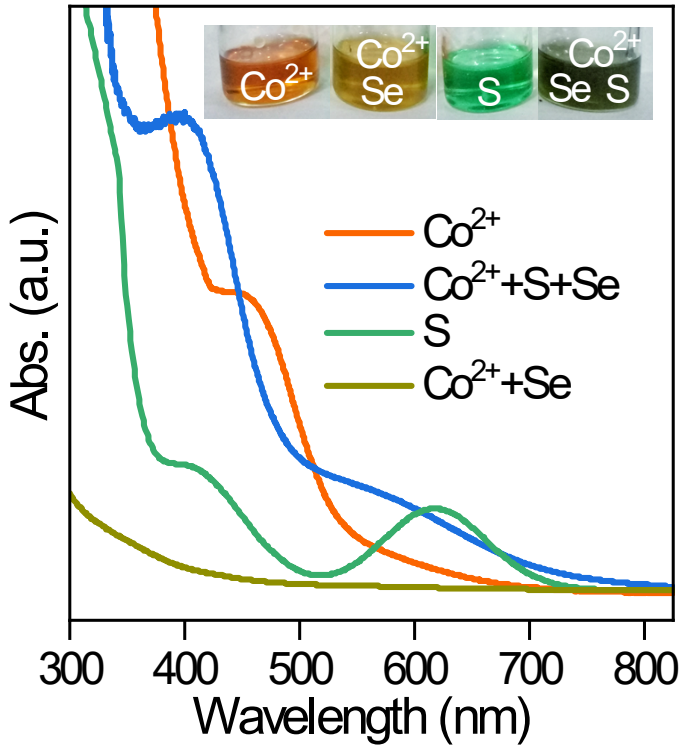

Figure S12. The UV-vis spectra of the precursor for the materials synthesis.

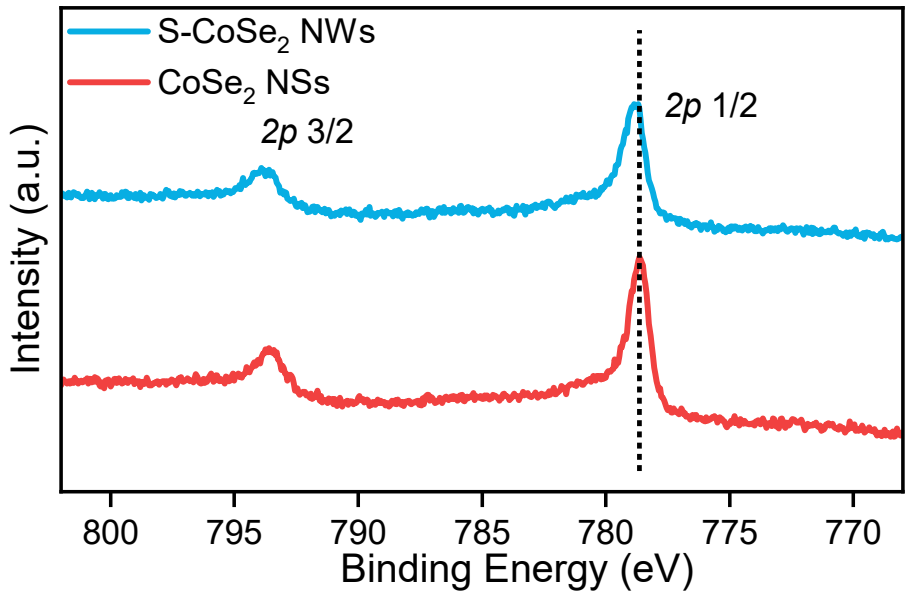

Figure S13. Co *2p* XPS spectra of $CoSe_2$ NSs and S-$CoSe_2$ NWs.

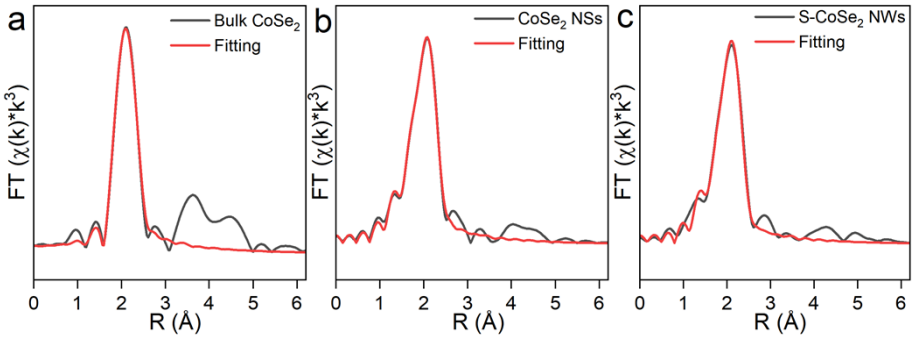

Figure S14. The EXAFS fitting for (a) Bulk $CoSe_2$, (b) $CoSe_2$ NSs and S-$CoSe_2$ NWs.

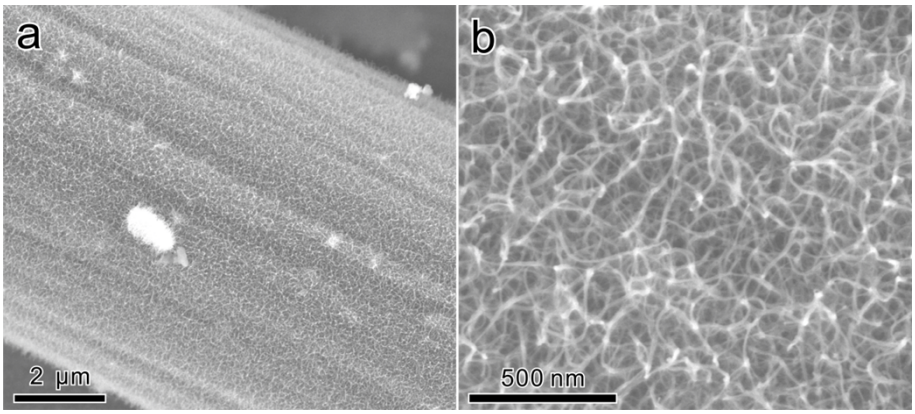

Figure S15. The SEM images of S-$CoSe_2$ NWs@CC with different magnification.

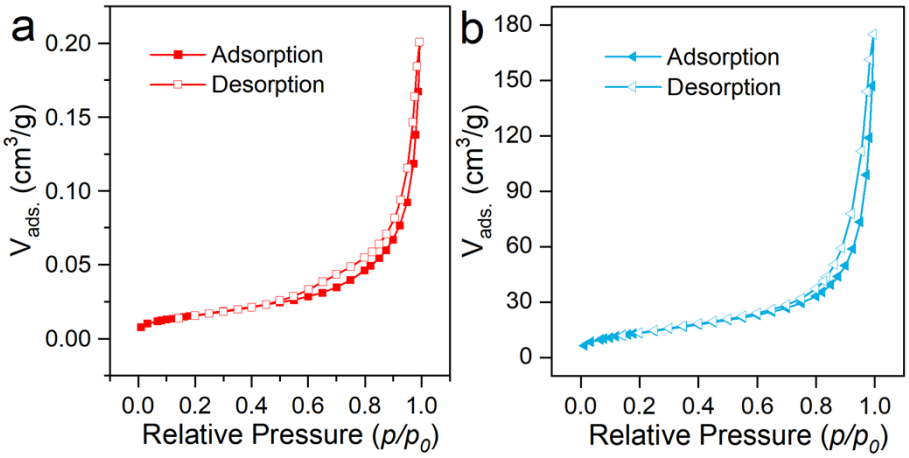

Figure S16. Nitrogen physisorption isotherms of (a) $CoSe_2$ NSs and (b) S-$CoSe_2$ NWs.

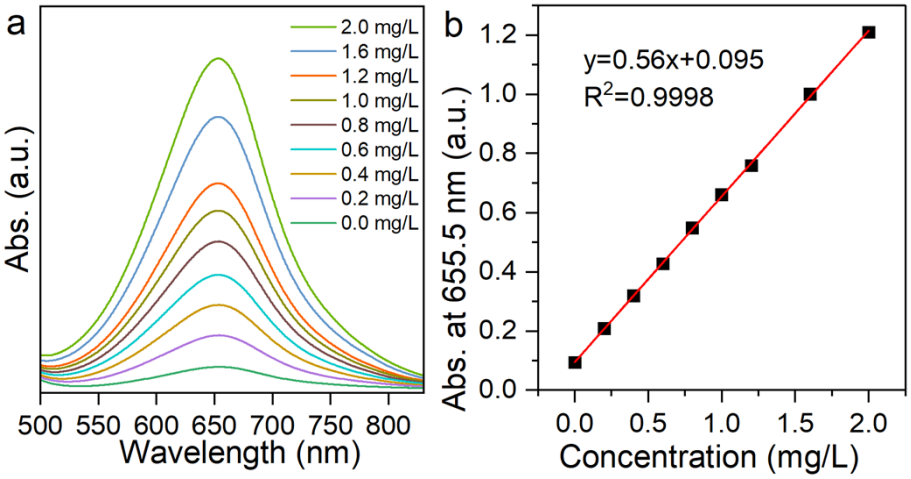

Figure S17. (a) UV-vis spectra with the absorbance of indophenol blue at 655.5 nm at different concentration of ammonium and (b) corresponding calibration curve used for NH_4^+ calculation.

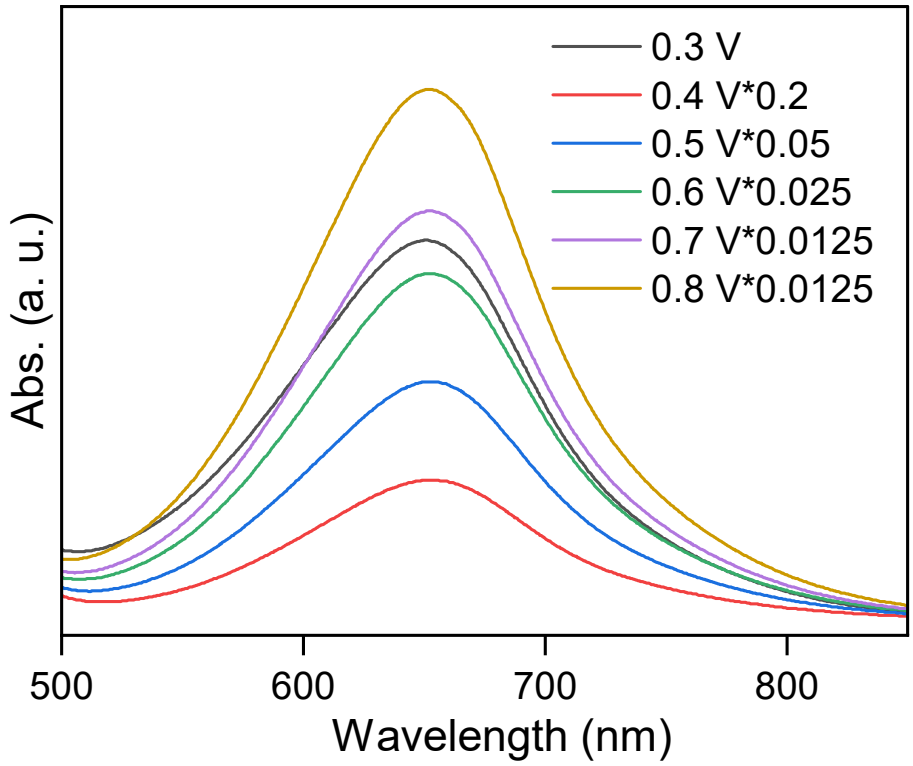

Figure S18. UV-vis spectra of electrolytes measured by the indophenol-blue method after NARR with S-$CoSe_2$ NWs. (The electrolyte has been diluted with different factors for testing.)

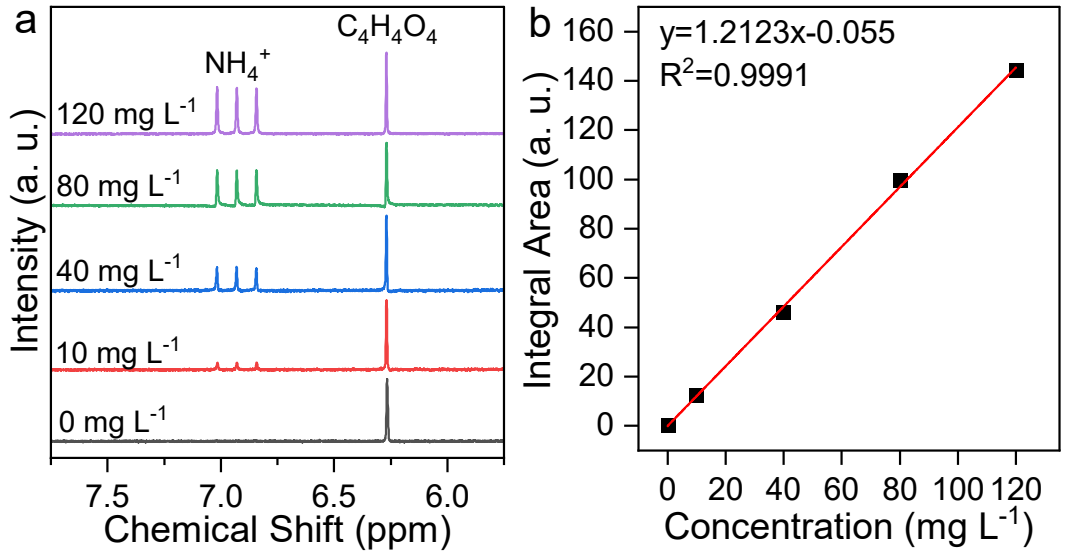

Figure S19. (a) ^1H NMR spectra of NH_4^+ at different concentrations using maleic acid as an internal standard and (b) corresponding NMR calibration curve for quantification of NH_4^+ in solution.

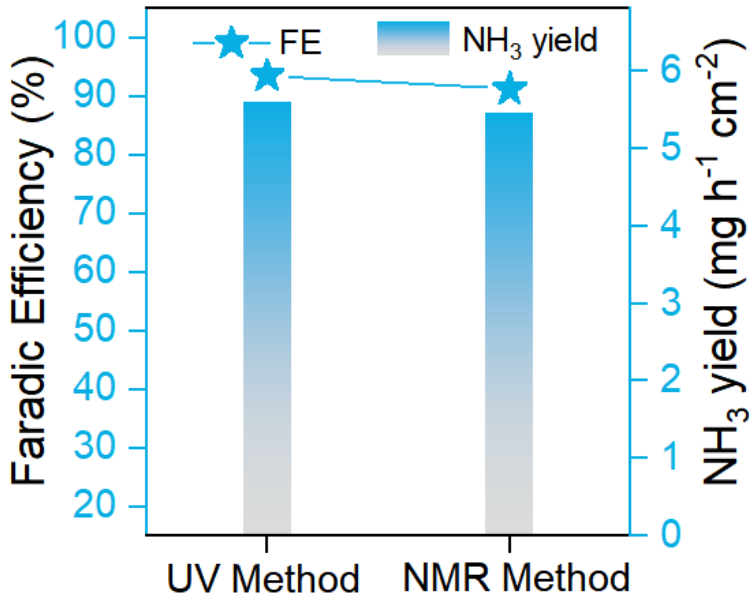

Figure S20. FE comparison between UV method and NMR method.

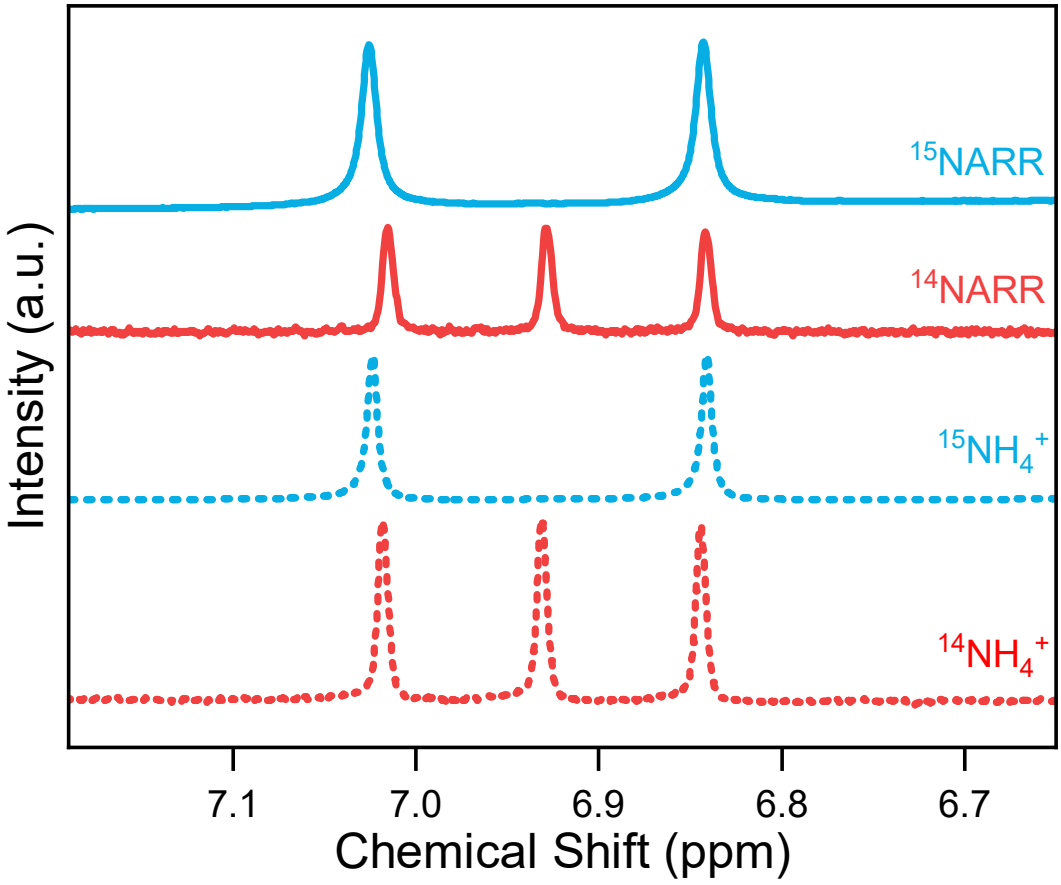

Figure S21. ^{1}H NMR spectra of standard samples and electrolytes after NARR with $^{14}NO_3^-$ and $^{15}NO_3^-$ as nitrogen source.

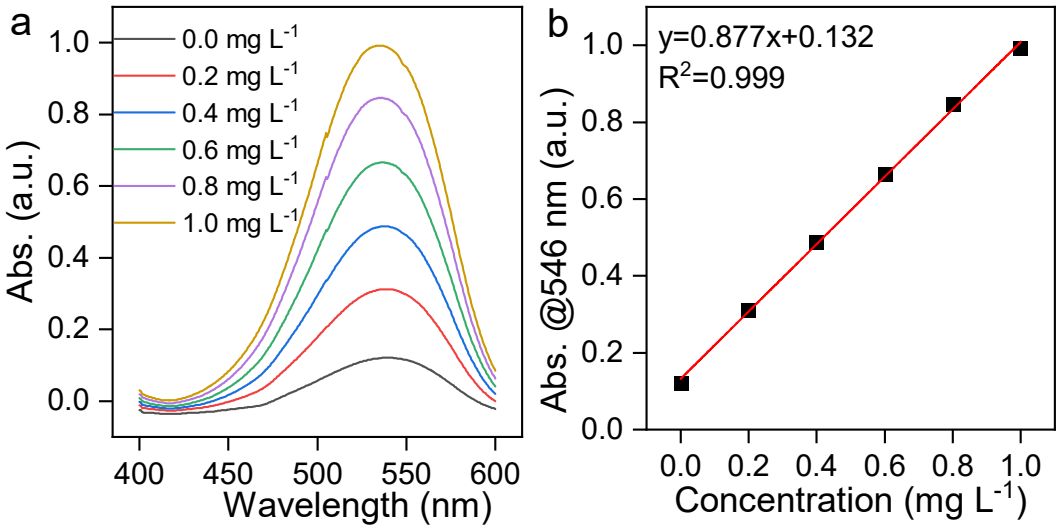

Figure S22. (a) UV-vis spectroscopy curves and (b) corresponding calibration curve used for NO_2^--N calculation.

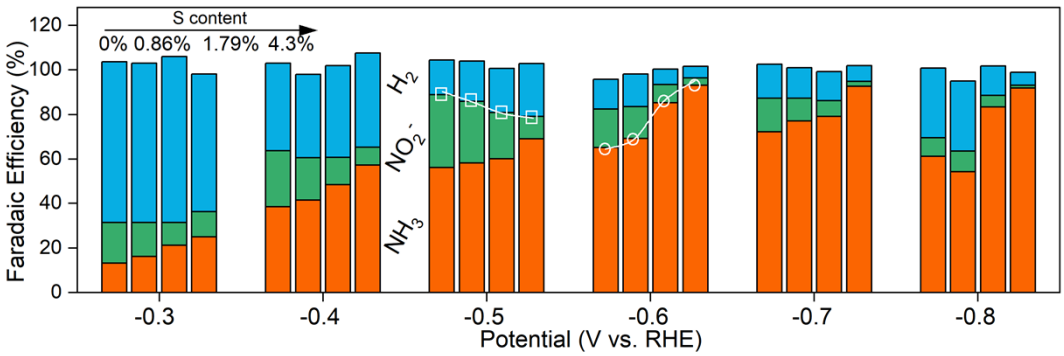

Figure S23. The FE collection of S-$CoSe_2$ materials at all given potentials.

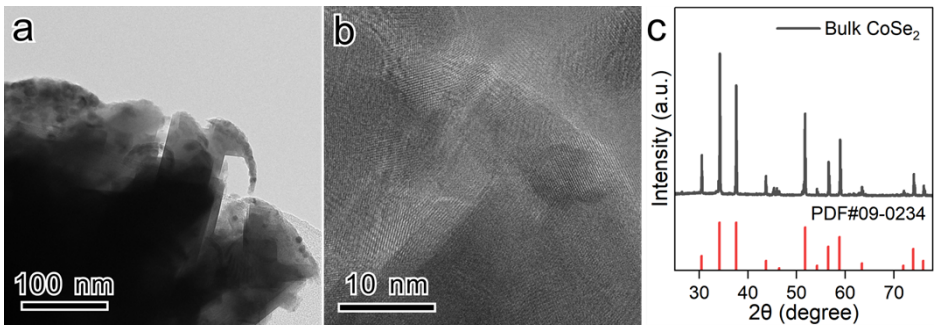

Figure S24. (a) TEM image, (b) HRTEM image and (c) XRD pattern of bulk $CoSe_2$.

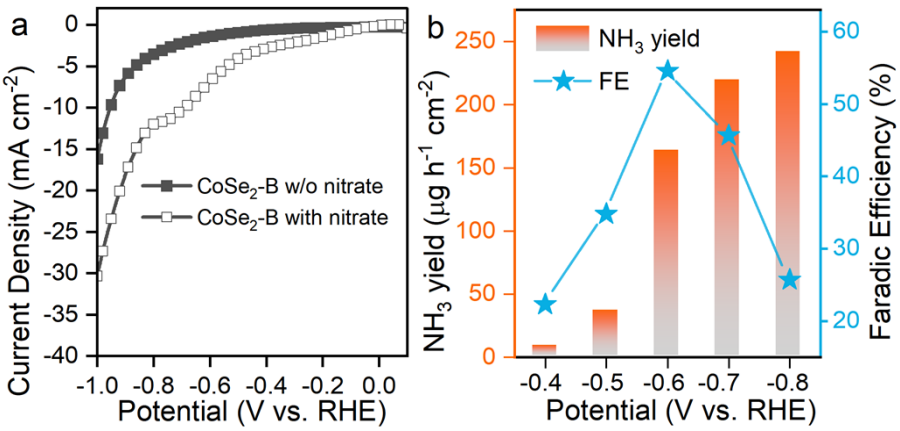

Figure S25. (a) LSV, (b) FE and NH_3 yield rate of bulk $CoSe_2$ at all given potentials.

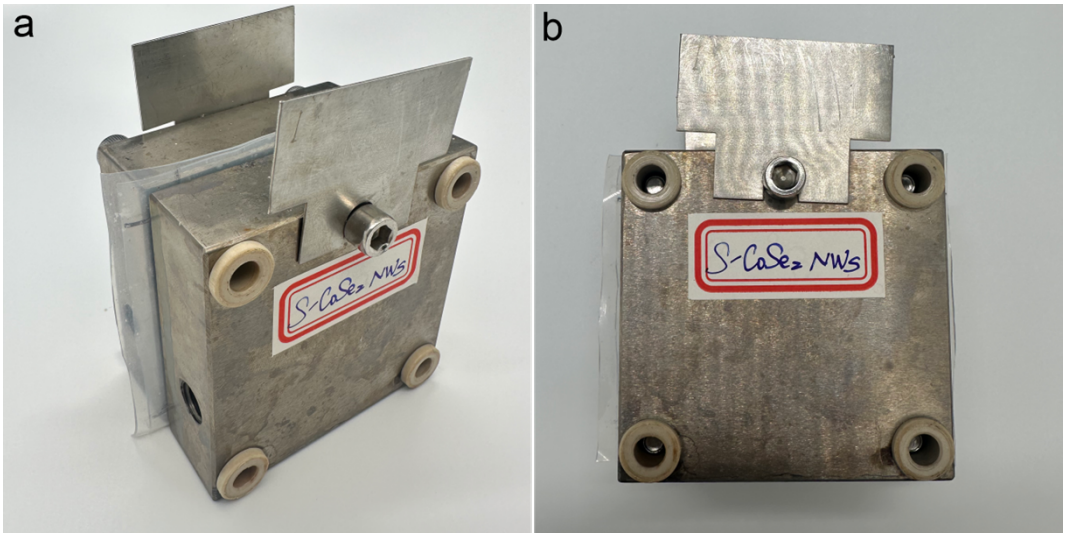

Figure S26. The (a) overhead view and (b) elevation view of the self-organized device NiFe LDH@Ni foam || S-$CoSe_2$ NWs@CC.

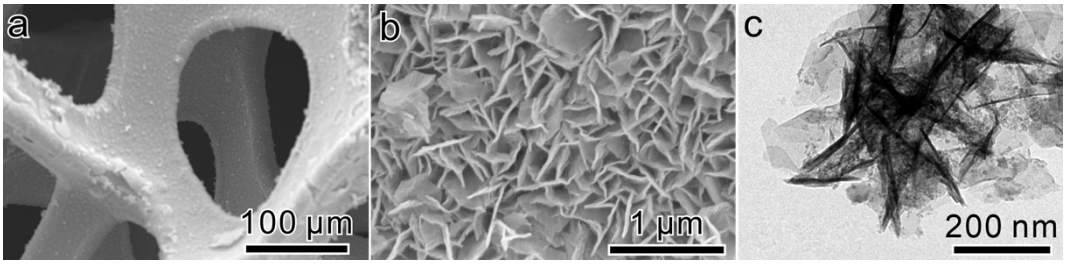

Figure S27. (a-b) SEM images of NiFe LDH@Ni foam with different magnification. (c) TEM image of NiFe LDH.

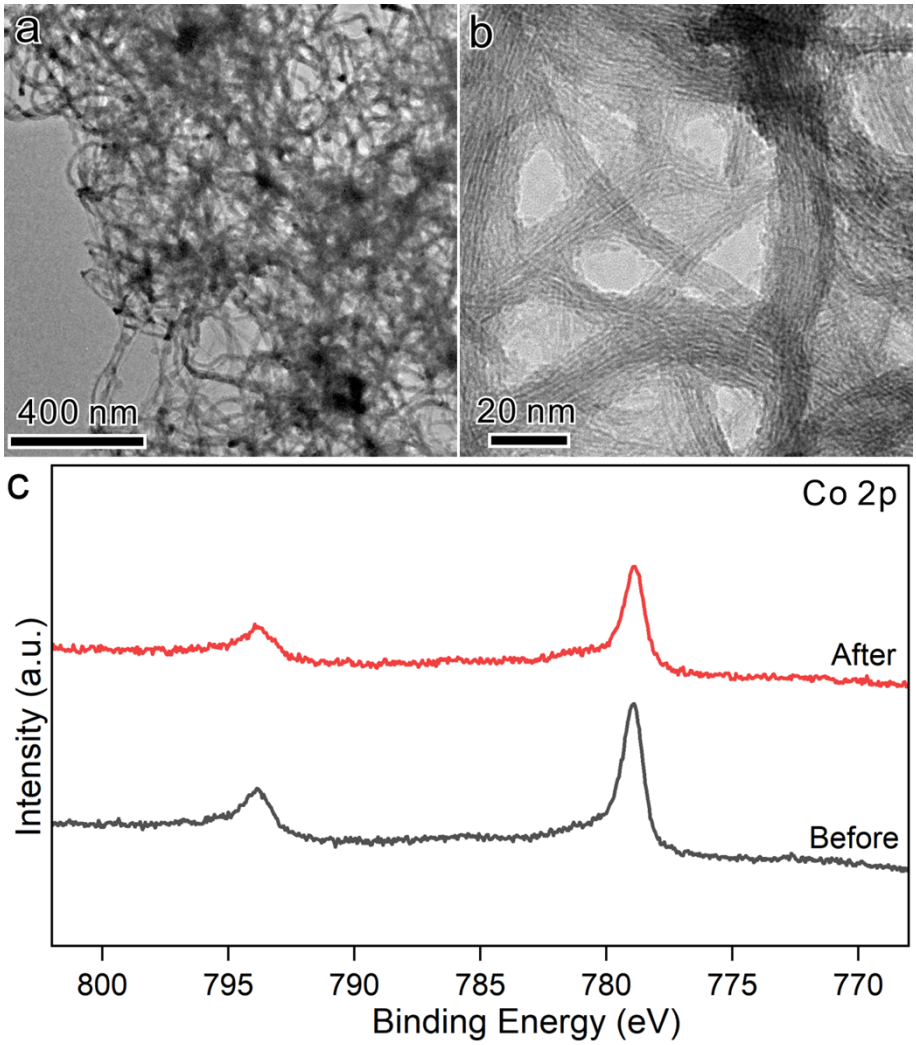

Figure S28. The (a) TEM image, (b) HRTEM and (c) Co *2p* XPS spectra of S-CoSe2 NWs after long-term reaction.

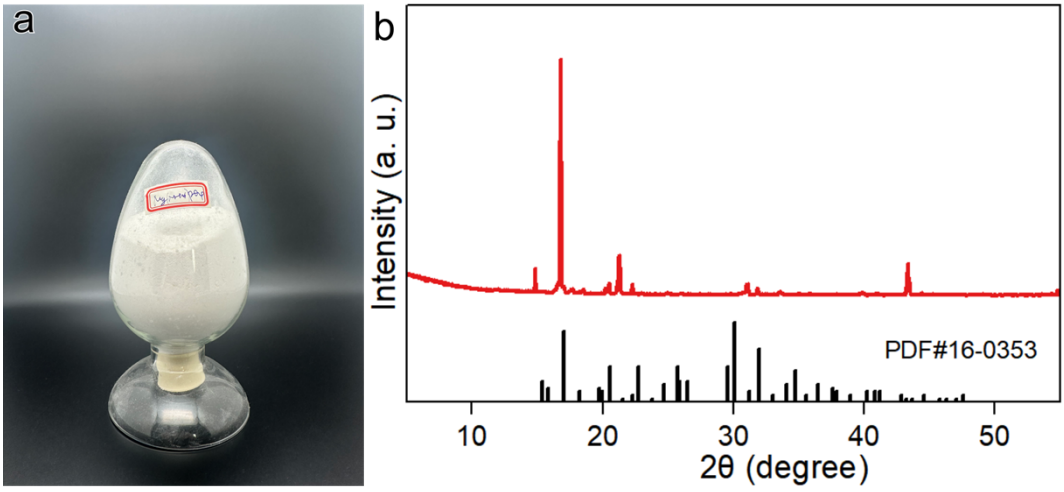

Figure S29. (a) optical image and (b) XRD pattern of struvite.

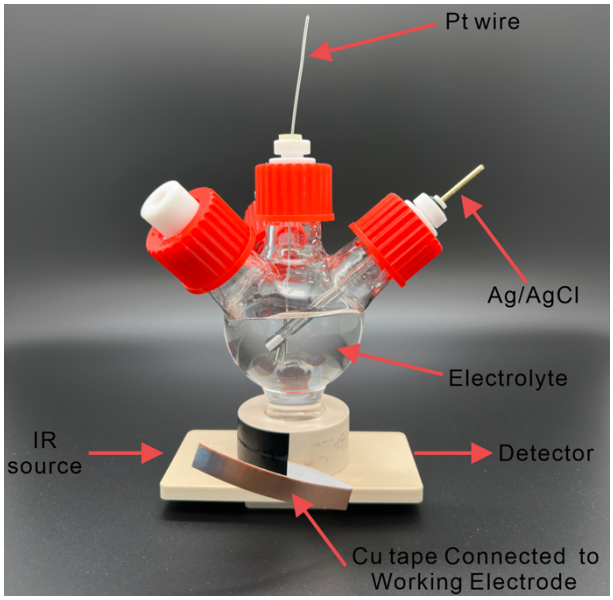

Figure S30. (a) optical image of electrochemical in-situ ATFTIR cell.

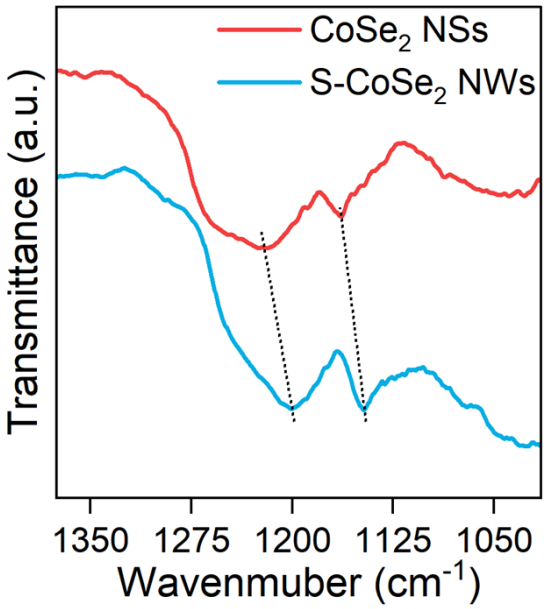

Figure S31. In-situ ATFTIR spectra of $CoSe_2$ NSs and S-$CoSe_2$ NWs at the potential of -0.6 V vs, RHE.

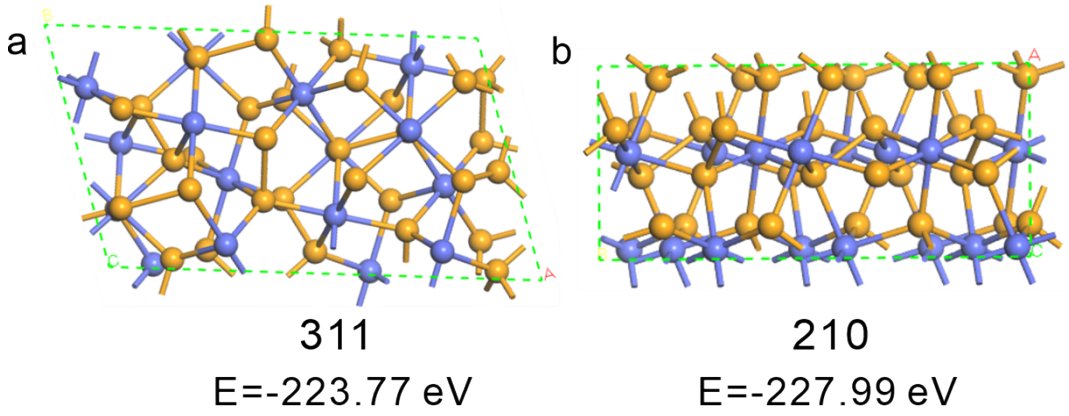

Figure S32. The surface energy for (a) 311 and (b) 210 facets of $CoSe_2$.

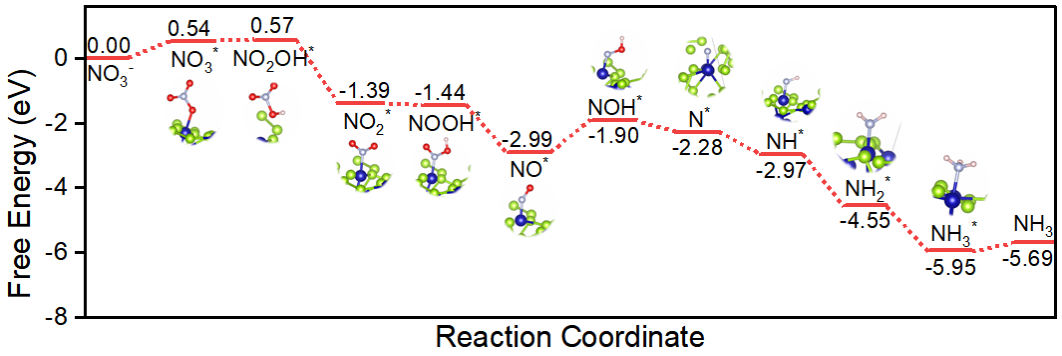

Figure S33. Reaction-free energies for different intermediates of NARR based on the model of $CoSe_2$.

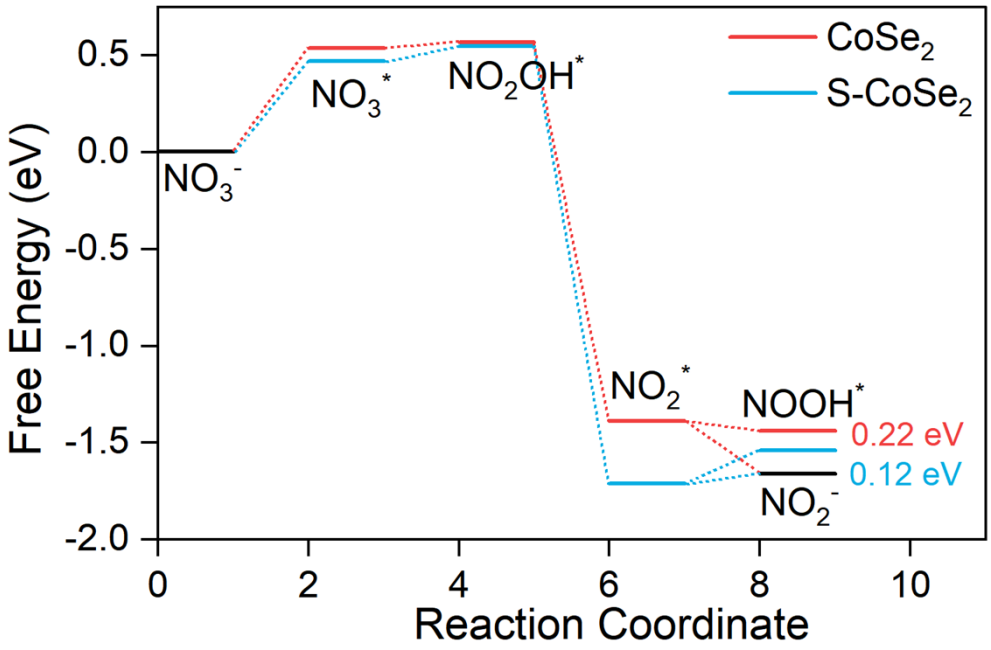

Figure S34. Reaction-free energies for different intermediates of NARR based on $CoSe_2$ and sulfur doped $CoSe_2$.

Table S1. EXAFS fitting parameters at the Co K-edge（S_0^2=0.68）

Sample	Path	C.N.	R (Å)	$\sigma^2\times10^3$ (Å^2)	ΔE (eV)	R factor
Bulk $CoSe_2$	Co-Se	6.3±0.4	2.42±0.01	6.0±4.3	-0.5±1.0	0.004
$CoSe_2$ NSs	Co-Se	6.1±0.8	2.37±0.01	6.0±1.0	-1.2±2.8	0.006
S-$CoSe_2$ NWs	Co-S	0.8±1.4	2.24±0.05	5.2±1.7	0.5±0.1	0.009
	Co-Se	4.5±1.0	2.40±0.01	6.6±1.3	2.4±0.5	

C.N.: coordination numbers; *R*: bond distance; σ^2: Debye-Waller factors; Δ*E*: the inner potential correction. *R* factor: goodness of fit. * fitting with fixed parameter.

Table S2. The elemental analysis results of $CoSe_2$ materials.

Sample	Weight [mg]	C/N ratio	Content [at%]
$CoSe_2$ NSs-1	1.58	0.732	N:0.482 H:0.353 S:0.021 H:0.191
$CoSe_2$ NSs-2	2.00	1.382	N:0.796 C:1.101 S:0.051 H:0.484
$CoSe_2$ NSs-3	4.48	2.400	N:0.903 C:2.167 S:0.061 H:0.431
S-$CoSe_2$ NWs-1	3.04	1.336	N:1.039 C:1.388 S:4.249 H:0.272
S-$CoSe_2$ NWs-2	4.26	1.602	N:1.067 C:1.709 S:3.982 H:0.259
S-$CoSe_2$ NWs-3	2.09	0.804	N:1.018 C:0.818 S:4.628 H:0.383

Reference

1. Y. Liu, H. Cheng, M. Lyu, S. Fan, Q. Liu, W. Zhang, Y. Zhi, C. Wang, C. Xiao, S. Wei, B. Ye and Y. Xie, *J. Am. Chem. Soc.*, 2014, **136**, 15670-15675.
2. C. Schlesiger, S. Praetz, R. Gnewkow, W. Malzer and B. Kanngiesser, *J. Anal. At. Spectrom.*, 2020, **35**, 2298-2304.
3. L. Zhou and C. E. Boyd, *Aquaculture*, 2016, **450**, 187-193.
4. Y. Wang, Y. Yu, R. Jia, C. Zhang and B. Zhang, *Natl. Sci. Rev.*, 2019, **6**, 730-738.

5. G. Kresse and J. Furthmuller, *Comput. Mater. Sci.*, 1996, **6**, 15-50.
6. P. E. Blöchl, *Phys. Rev. B*, 1994, **50**, 17953-17979.
7. J. P. Perdew, J. A. Chevary, S. H. Vosko, K. A. Jackson, M. R. Pederson, D. J. Singh and C. Fiolhais, *Phys. Rev. B*, 1992, **46**, 6671-6687.
8. H.-F. Wang and Z.-P. Liu, *J. Am. Chem. Soc.*, 2008, **130**, 10996-11004.
9. C. Guo, X. Tian, X. Fu, G. Qin, J. Long, H. Li, H. Jing, Y. Zhou and J. Xiao, *ACS Catal.*, 2022, **12**, 6781-6793.